Molecular Profiling of Neurons Based on Connectivity

Mats I. Ekstrand,[1,2] Alexander R. Nectow,[1,2] Zachary A. Knight,[1] Kaamashri N. Latcha,[1] Lisa E. Pomeranz,[1] and Jeffrey M. Friedman[1,*]
[1]Laboratory of Molecular Genetics, Howard Hughes Medical Institute, The Rockefeller University, 1230 York Avenue, New York, NY 10065, USA
[2]Co-first authors
*Correspondence: friedj@rockefeller.edu
http://dx.doi.org/10.1016/j.cell.2014.03.059

SUMMARY

The complexity and cellular heterogeneity of neural circuitry presents a major challenge to understanding the role of discrete neural populations in controlling behavior. While neuroanatomical methods enable high-resolution mapping of neural circuitry, these approaches do not allow systematic molecular profiling of neurons based on their connectivity. Here, we report the development of an approach for molecularly profiling projective neurons. We show that ribosomes can be tagged with a camelid nanobody raised against GFP and that this system can be engineered to selectively capture translating mRNAs from neurons retrogradely labeled with GFP. Using this system, we profiled neurons projecting to the nucleus accumbens. We then used an AAV to selectively profile midbrain dopamine neurons projecting to the nucleus accumbens. By comparing the captured mRNAs from each experiment, we identified a number of markers specific to VTA dopaminergic projection neurons. The current method provides a means for profiling neurons based on their projections.

INTRODUCTION

An important goal in neuroscience is to understand how neural circuits control behavior. Toward this end, intensive efforts are being made to delineate the complete wiring diagram, or connectome, of the mammalian brain. High-throughput electron microscopy has been used to define microscale connectivity (Helmstaedter et al., 2013), while tracing strategies utilizing virally encoded fluorophores have allowed for milliscale circuit mapping (Wickersham et al., 2007), with postsynaptic cell-type specificity in some cases (Wall et al., 2010; Wall et al., 2013). While these studies have elegantly dissected a number of complex circuits, they are not designed to provide molecular information about the presynaptic neural populations. The identification of marker genes for neurons comprising circuits enables testing of their functional role, which is key to understanding how the brain controls complex neural processes.

Methods for identifying markers expressed in molecularly defined neurons in the mammalian nervous system have been developed by translationally profiling cells through the expression of a ribosomal tag (Heiman et al., 2008; Sanz et al., 2009). Translating ribosome affinity purification (TRAP) can yield molecular profiles of defined neural populations using cell-type-specific expression of a GFP-L10 fusion protein through bacterial artificial chromosome (BAC) transgenesis or conditional expression of a floxed allele (Doyle et al., 2008; Stanley et al., 2013).

While providing detailed information about the molecular identity of populations of neurons, TRAP does not provide neuroanatomical information. Given that the function of a defined population of neurons is inextricably linked to its circuit connectivity, we sought to adapt TRAP technology to molecularly profile and identify subsets of neurons that project into specific brain regions. We focused first on the nucleus accumbens, which plays an important role in diverse behaviors such as feeding, addiction, and depression (Chaudhury et al., 2013; Lim et al., 2012; Lüscher and Malenka, 2011; Tye et al., 2013).

To profile neurons based on their site of projection, we set out to functionalize green fluorescent protein (GFP) (Tsien, 1998), such that it could tag ribosomes and allow their precipitation in a manner analogous to that of TRAP. Since GFP is commonly encoded in retrograde tracing viruses, such as canine adenovirus type 2 (CAV; Bru et al., 2010), this approach would allow us to precipitate ribosomes from only those neurons that project to a defined region. To achieve this, we utilized camelid nanobodies, which are small, genetically encoded, intracellularly stable and bind their antigens with high specificity and avidity (Muyldermans, 2013). Camelid nanobodies have recently been used in a number of applications, such as intracellular localization of proteins (Ries et al., 2012), live-cell antigen targeting (Rothbauer et al., 2006), and modulation of gene expression (Tang et al., 2013).

We hypothesized that an anti-GFP nanobody fused to a ribosomal protein could stably bind GFP intracellularly and allow for ribosome precipitation. Moreover, if used in combination with GFP expressed from a retrograde tracing virus such as CAV-GFP, this approach would allow for immunoprecipitation of ribosomes specifically from projective neurons.

In the current work, we generated transgenic mice that express an N-terminal fusion protein consisting of the V_HH fragment of a camelid antibody raised against GFP (Rothbauer et al., 2006), fused to large ribosomal subunit protein Rpl10a (NBL10)

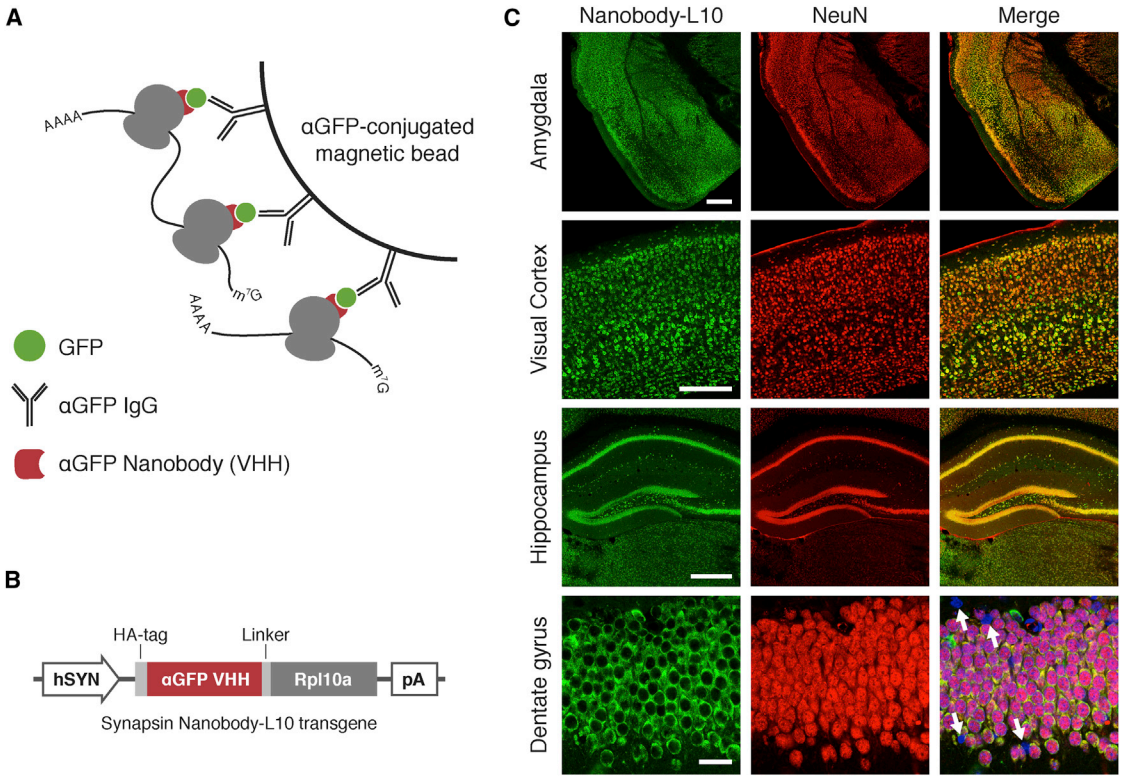

Figure 1. Neuron-Specific Expression of a Nanobody-L10 Fusion Protein

(A) Heterologous expression of an anti-GFP camelid nanobody fused to a ribosomal protein allows for immunoprecipitation of translating mRNAs in the presence of GFP.

(B) Transgene used to generate SYN-NBL10 mice. A neuron-specific human synapsin promoter (SYN) drives the expression of an HA-tagged anti-GFP camelid VHH domain (nanobody) fused to ribosomal protein L10a.

(C) Colocalization between HA-tagged NBL10 (green) and neuronal marker NeuN (red) in various brain regions. Dentate gyrus merge also displays Hoechst staining to show the presence of HA-/NeuN- glial cell-types (white arrows).

Scale bars, 500 μm for amygdala and hippocampus, 250 μm for visual cortex, and 25 μm for dentate gyrus. See also Figure S1.

under the control of the synapsin promoter. By injecting the retrogradely transported CAV-GFP virus (Bru et al., 2010) into the nucleus accumbens shell, we were able to capture ribosomes from presynaptic neurons in the ventral midbrain and hypothalamus, and identify markers delineating cell-types that project to this region. Furthermore, using a Cre-conditional AAV encoding the NBL10 fusion, we were able to molecularly profile VTA dopamine neurons projecting to the nucleus accumbens. This work provides a general means for molecularly profiling presynaptic cell-types based on their projection pattern, and identifies marker genes for neuronal populations that are potentially relevant to a variety of behaviors including feeding, and neuropsychiatric diseases, such as addiction and depression.

RESULTS

Generation of SYN-NBL10 Transgenic Mice

GFP is commonly used to visualize restricted subsets of neurons within the brain, but means for directly profiling these neurons are limited (Sugino et al., 2006). In order to profile neurons expressing GFP, we first set out to tag ribosomes with a camelid nanobody raised against GFP (Figure 1A). Previous work has demonstrated that it is possible to create N-terminal fusions of the large ribosomal subunit protein Rpl10a with small epitope tags such as GFP that do not interfere with ribosome function (Heiman et al., 2008). We thus generated a transgenic mouse that expresses an anti-GFP nanobody fused to the N terminus of ribosomal subunit protein Rpl10a (NBL10) under the control of the neuron-specific human synapsin promoter (hereafter SYN-NBL10). In addition, we engineered the NBL10 fusion protein with an HA tag, allowing us to visualize the sites of expression using immunohistochemistry (Figure 1B).

To confirm that expression of the NBL10 transgene was neuron-specific, we performed immunohistochemistry for HA and NeuN, a commonly used neuronal marker (Figure 1C). We then counted more than 4,000 cells (n = 3 mice) and found only 4 cells that were not double-labeled, demonstrating that NBL10 expression is neuron-specific in these mice (Figure S1 available online). Moreover, upon counterstaining with Hoechst to mark all nuclei in the brain, we found large numbers of HA-/NeuN- cells, further indicating that NBL10 is not expressed in nonneuronal cell-types (Figure 1C, white arrows).

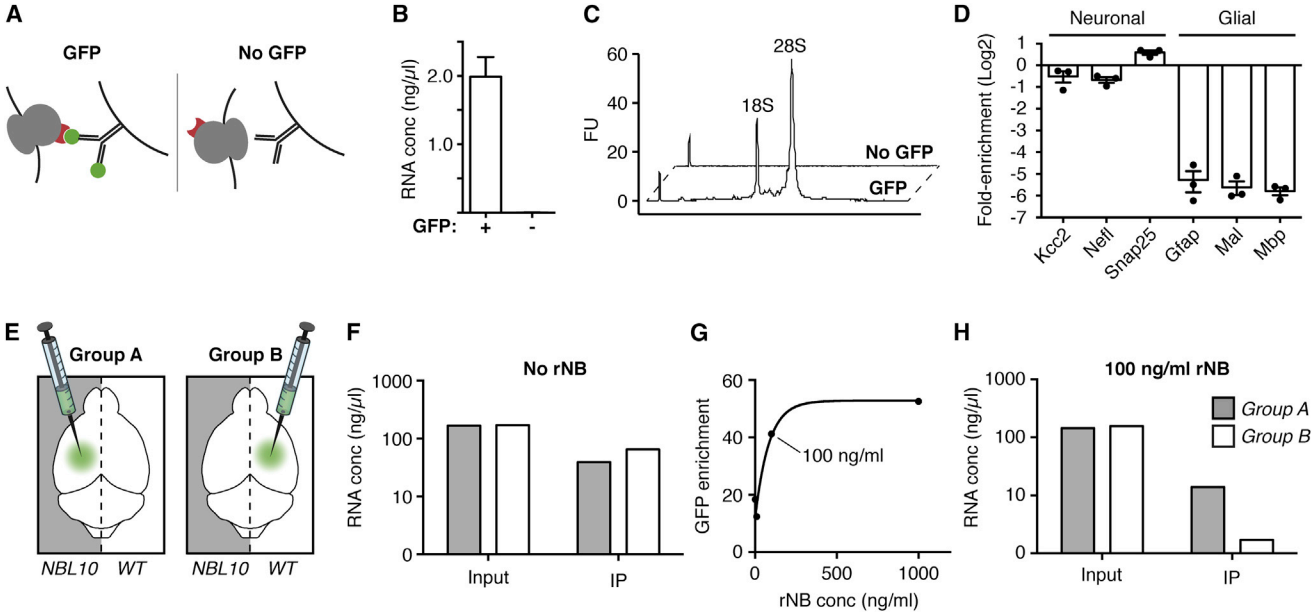

Figure 2. Optimization of Immunoprecipitation for GFP

(A) Schematic of immunoprecipitation with beads with and without GFP.

(B) Quantification of RNA yield after immunoprecipitation from SYN-NBL10 mice using GFP-coated or uncoated magnetic beads ($p < 0.01$).

(C) Bioanalyzer trace of immunoprecipitated RNA with and without GFP. FU, fluorescence units.

(D) Taqman analysis of neuronal and glial marker genes in RNA immunoprecipitated with recombinant GFP ($p < 0.0001$ for glial markers).

(E) Mixing experiment illustration. CAV-GFP is injected into a SYN-NBL10 (gray background) or wild-type (white background) mouse. Injected brains are homogenized together with a noninjected brain of the complementary genotype to assay GFP-nanobody binding in lysates during the IP.

(F) RNA yield after immunoprecipitation of mixed lysates with no recombinant nanobody (rNB) added to the homogenization buffer.

(G) GFP enrichment in IP RNA from SYN-NBL10 mice injected with CAV-GFP. Data are plotted as GFP fold enrichment (IP/Input) against buffer rNB concentration.

(H) RNA yield after immunoprecipitation of mixed lysates with 100 ng/ml rNB in the buffer.

Data are presented as mean ± SEM. See also Figure S2.

Nanobody-Tagged Ribosomes Can Be Precipitated Using GFP

We next set out to selectively immunoprecipitate (IP) neuronal ribosomes from SYN-NBL10 transgenic mice using GFP. Magnetic beads were coated with anti-GFP monoclonal antibodies that bind different epitopes on GFP than the one recognized by the nanobody. We then compared the ability of beads loaded with recombinant GFP versus control beads to immunoprecipitate ribosomes from whole-brain lysate of SYN-NBL10 transgenic mice (Figure 2A). In our immunoprecipitate, we obtained yields of 2.0 ng/μl RNA for GFP-loaded beads and 0.004 ng/μl RNA for control beads ($p < 0.01$; Figure 2B). Similarly, 18S and 28S rRNA peaks were only detected in IPs using GFP-coated beads demonstrating that GFP is required for immunoprecipitation of RNA (Figure 2C). If the IP is specific to neuronal ribosomes, we would also expect to substantially deplete for glial markers, while not depleting for neuronal markers in the precipitated RNA. We found that RNA for all tested glial markers were indeed depleted in the IP relative to total (Input) RNA: *Gfap* (38.8-fold), *Mal* (49.1-fold), and *Mbp* (55.1-fold) ($p < 0.0001$ for all genes; Figure 2D). As expected, the neuronal markers *Kcc2*, *Nefl*, and *Snap25*, were present in similar amounts in the IP relative to Input RNA. All enrichments were determined by dividing IP over Input values for each gene after normalization to Rpl23. These experiments confirmed that nanobody-tagged neuronal ribosomes can be selectively immunoprecipitated from SYN-NBL10 transgenic mice in the presence of GFP, while immunoprecipitation of glial ribosomes is markedly reduced.

Selective Immunoprecipitation of Ribosomes Bound to Virally Encoded GFP

The finding that GFP can be used to immunoprecipitate NBL10-decorated ribosomes suggested that this approach could be used to precipitate ribosomes after infection of neurons with a virus expressing GFP. Canine adenovirus expressing GFP (CAV-GFP) was injected bilaterally into the nucleus accumbens (Figure S2A), and the region surrounding the injection site was dissected. Immunohistological staining revealed that the vast majority of cells that were infected were neurons (Figure S2D). We then lysed tissue from the infected region and performed a GFP IP (Figure S2B). Consistent with the previous data, glial markers were depleted: *Gfap* (11.1-fold), *Mal* (14.8-fold), and *Mbp* (21.2-fold). In addition, *Gfp* was enriched (11.5-fold; Figure S2C). To test the possibility that GFP enrichment might be artificially increased by directly pulling down the nascent translating strand, we infected Hepa 1-6 cells with CAV-GFP (Figure S2E) and performed IPs. In this case, we were not able to detect any RNA in our IPs (Figures S2F and S2G), demonstrating that nascent strand

contamination of our IPs is negligible. Additionally, we observed no substantial alterations in endogenous gene expression relative to mock infected cells, further confirming that CAV-GFP is a suitable virus for translational profiling (Figure S2H).

However, since only virally infected cells should express GFP mRNA, we had expected to obtain a substantially higher enrichment for GFP above the 11.5-fold that was observed. We thus considered the possibility that *Gfp* enrichment might be lower than expected due to viral overexpression of GFP. Excess GFP would likely have a high stoichiometry relative to the NBL10 fusion protein, in which case there might not be enough nanobody to sequester all soluble GFP protein in infected cells, leading to GFP spillover in the lysate. Spillover would potentially cause promiscuous GFP binding to free NBL10-labeled ribosomes from nearby but uninfected neurons. This would, in turn, lead to a decrease in the relative amount of GFP RNA in our IPs and consequently reduce enrichment of GFP RNA as well as other mRNAs expressed in the infected neurons. We addressed this possibility by designing a mixing experiment to test whether GFP spillover was a significant source of background.

The mixing experiment was designed to assess the extent to which excess GFP could bind to nanobody-tagged ribosomes after tissue homogenization. In a first experiment, tissue from wild-type (WT) mice infected with CAV-GFP was combined with tissue from uninfected SYN-NBL10 transgenic mice and homogenized together (hereafter group B; Figure 2E, right). If RNA was precipitated after incubation of the mixed lysate with magnetic beads coated with anti-GFP antibodies, it would confirm that free GFP was binding to nanobody-labeled ribosomes after tissue homogenization. The data were compared to that in which tissue from CAV-GFP-infected SYN-NBL10 transgenic mice was mixed with tissue from WT mice (group A; Figure 2E, left). We found that equivalent amounts of RNA were precipitated in groups A and B thus confirming that free GFP can bind to nanobody-labeled ribosomes in the lysate (Figure 2F). This suggested that a robust experiment would require the elimination of this binding.

We reasoned that by adding recombinant nanobody (rNB) to the lysate, we could sequester free GFP and render it unavailable for binding to the NBL10 fusion protein. This would reduce the background in our immunoprecipitate and thus augment GFP enrichment. To test this, we analyzed the fold enrichment for GFP RNA in immunoprecipitations from brains of CAV-GFP-infected SYN-NBL10 mice in the presence of increasing amounts of rNB in the homogenization buffer. We found that the addition of rNB markedly increased the fold enrichment for GFP RNA to more than 41-fold, compared to the previously observed 11.5-fold enrichment without the addition of rNB (Figure 2G). We also found that the increased enrichment of GFP RNA was near maximal at 100 ng/ml of added rNB (Figure 2G).

We then repeated the mixing experiment described above, now adding 100 ng/ml of rNB prior to tissue homogenization. In this case, substantially more RNA was recovered from group A (~14 ng/μl), as compared to group B (1.7 ng/μl; Figure 2H). These data demonstrate that the addition of 100 ng/ml of free rNB is sufficient to reduce promiscuous binding of GFP to ribosomes from uninfected neurons, while also maximizing the enrichment of GFP. Thus, the addition of recombinant nanobody prior to tissue homogenization greatly improves the specificity of the GFP immunoprecipitation.

Translational Profiling of Neurons Projecting to the Nucleus Accumbens

The previous experiments demonstrated that we are able to immunoprecipitate ribosomes specifically from CAV-GFP-infected neurons in SYN-NBL10 transgenic mice. We next set out to molecularly profile neurons that project from one region to another by exploiting the retrograde transport of CAV-GFP from nerve terminals to soma. This virus is replication deficient, so when it reaches the soma of the presynaptic neuron, it is incapable of traversing synapses and will not infect any other upstream neurons. Thus by infecting nerve terminals with CAV-GFP in SYN-NBL10 transgenic mice, ribosomes in the soma will be labeled with GFP. We next assessed whether we could isolate ribosomes and mRNA from neurons that project into the nucleus accumbens (NAc).

The nucleus accumbens integrates inputs from diverse regions throughout the brain, including the raphe nuclei in the brainstem, the medial prefrontal cortex, and hippocampus. Additionally, the NAc receives heavy input from dopaminergic neurons of the ventral tegmental area (VTA), as well as inputs from melanin-concentrating hormone (MCH) neurons of the lateral hypothalamus (LH; Georgescu et al., 2005). These populations are known to play important roles in reward-related behaviors and feeding, respectively. We were especially interested in these circuits because dysfunction of the NAc can contribute to a variety of disorders, such as obesity, addiction, and depression. Importantly, the VTA and LH inputs are anatomically segregated (i.e., sufficiently distant) from the accumbens shell, making it possible to dissect the brain regions from which these presynaptic populations originate without contaminating our IP with CAV-GFP-infected neurons at the site of injection (Figure 3A). While subsets of MCH neurons of the LH and dopaminergic neurons of the VTA project to regions other than the NAc, the current methodology would allow us to selectively profile only the subpopulations of MCH and DA neurons that project directly to the accumbens shell. Neurons that do not project to the NAc will not express GFP, and their ribosomes will therefore not be precipitated (Figure 3B).

We injected mice with CAV-GFP in the nucleus accumbens and mapped the regions that were labeled with GFP to visualize neurons that project to the NAc. We observed a large number of GFP-positive neurons throughout the midbrain and hypothalamus (Figure 3C), as well as in the medial prefrontal cortex, amygdala, hippocampus, and dorsal raphe nucleus (Figure S3). Consistent with previous reports (Lammel et al., 2011), we also found that the majority of VTA neurons retrogradely labeled from the nucleus accumbens expressed tyrosine hydroxylase (TH; Figure 3D), a marker for dopaminergic neurons. We observed substantial numbers of GFP-positive neurons in the hypothalamus and confirmed that GFP colocalized with MCH in a subset of neurons in the LH (Figure 3E).

To purify ribosomes from neurons projecting to the NAc, we dissected a 3 mm piece of tissue distant from the site of injection that included the hypothalamus and the midbrain after bilateral injections of CAV-GFP in the NAc of SYN-NBL10 mice. We

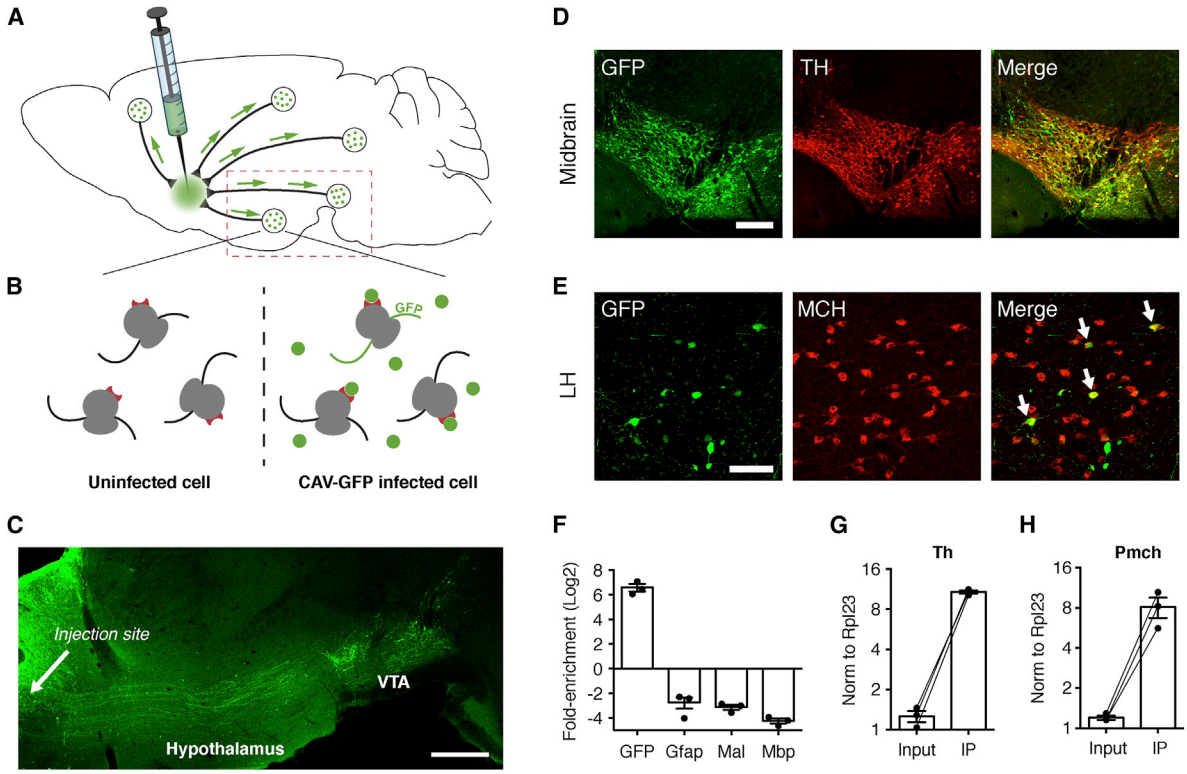

Figure 3. Projection-Specific Translational Profiling after CAV-GFP Injections into Nucleus Accumbens

(A) CAV-GFP injected into the nucleus accumbens is retrogradely transported to brain regions that send projections to the injection site. Only projective neurons will express GFP, as the virus is unable to replicate or cross synapses. Dashed red box indicates dissection for immunoprecipitation.

(B) Infected neurons contain GFP mRNA and protein (green circles) that can bind nanobody-tagged (red) ribosomes. Interspersed uninfected cells will not contain GFP mRNA or protein.

(C) Sagittal image showing retrograde spread of CAV-GFP through the hypothalamus and ventral midbrain.

(D) Colocalization between GFP and TH in the ventral midbrain.

(E) Colocalization between GFP and MCH in the lateral hypothalamus. White arrows indicate double-positive cells.

(F) qPCR for GFP and glial transcripts after IP ($p < 0.05$ for all genes). Data are expressed as fold enrichment (IP RNA/Input RNA).

(G and H) qPCR results for tyrosine hydroxylase ($p < 0.001$) and pro-melanin-concentrating hormone ($p < 0.05$) transcripts.

Scale bars, 500 μm in (C), 250 μm in (D), and 100 μm in (E). qPCR data are normalized to Rpl23 expression. Data are presented as mean ± SEM. See also Figure S3.

performed GFP IPs in the presence of 100 ng/ml rNB (Figure 3A, red dashed box). We observed highly significant enrichment for *Gfp* RNA (96.4-fold), while depleting for all glial markers tested: *Gfap* (6.7-fold), *Mal* (8.7-fold), and *Mbp* (18.8-fold) ($p < 0.05$ for all genes; Figure 3F). Importantly, we found significant enrichment for *Th* RNA (8.7-fold, $p < 0.001$; Figure 3G) and *Pmch* RNA (6.7-fold, $p < 0.05$; Figure 3H). These data validate that the current method can identify marker genes for neurons that project to the NAc.

Identification of Marker Genes for Neurons Projecting to the Nucleus Accumbens

Dopaminergic neurons of the VTA (Sesack and Grace, 2010) and MCH neurons of the LH (Georgescu et al., 2005) are known to project to the nucleus accumbens. However, the molecular profile of the specific subsets of these neurons that project to the NAc has not been explored, nor have markers for additional neural populations that project to this region been systematically identified. To address this, we performed high-throughput RNA sequencing (RNA-seq) on the IP RNA, as well as on the Input RNA from the midbrain and hypothalamus after injection of CAV-GFP into the NAc of SYN-NBL10 mice (Figures 4A and 4B). The total number of mapped reads was similar between the Input and IP RNA samples. Analysis of the sequencing data showed significant enrichment (IP/Input) of greater than 100-fold for GFP (Figure 4A), suggesting that the IP was highly specific for CAV-GFP-infected neurons that project from the dissected region to the NAc.

We plotted the IP RNA and Input RNA FPKM (fragment per kilobase of transcript per million mapped reads) values on a log-log scale (Figure 4C). The top 75 genes that were enriched in the IP RNA samples after RNA-seq analysis are also listed in Table S1. As seen previously with qPCR, RNA-seq data showed enrichment for *Pmch* (6.9-fold), as well as *Tacr3* (6.5-fold) and *Cartpt* (5.1-fold), and transcription factors *Foxa1* (5.7-fold) and *Foxa2* (4.9-fold). All of these genes have been reported to be coexpressed in MCH neurons (Croizier et al., 2010; Knight et al., 2012; Silva et al., 2009).

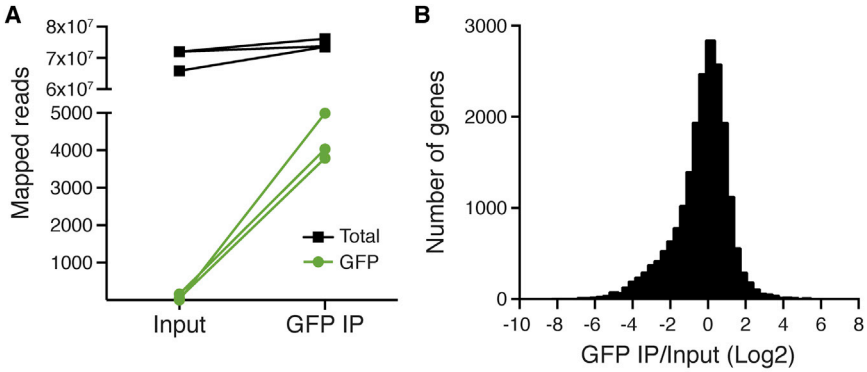

Figure 4. Identification of Differentially Expressed Marker Genes by RNA-Seq

(A) RNA-seq analysis of total reads mapped to the mouse genome (black) and EGFP-coding sequence (green) plotted on a linear scale.

(B) Histogram display of number of differentially enriched genes (IP/Input).

(C) FPKM GFP IP plotted against FPKM Input on a log-log scale. Outer lines are 2-fold enriched/depleted genes. A subset of differentially enriched marker genes are highlighted. Red dots indicate genes that are significantly different ($q < 0.05$) in Input versus IP. Blue dots indicate nonsignificant genes.

See also Table S1 and Figure S4.

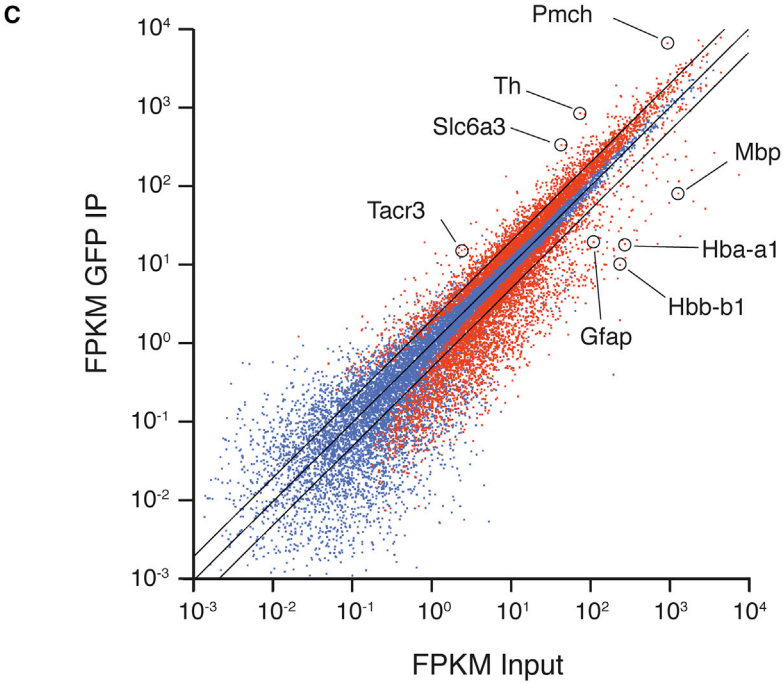

Similarly, marker genes coexpressed with *Th* (11.4-fold enriched) in dopaminergic neurons of the ventral midbrain were also enriched including, *Slc6a3* (7.8-fold), *Ddc* (5.2-fold), and *Nurr1* (5.2-fold), as well as α-synuclein (*Snca*, 4.9-fold; Mosharov et al., 2009). These genes were then reconfirmed with qPCR: *Slc6a3* (10.1-fold, $p < 0.05$), *Ddc* (5.7-fold, $p < 0.01$), *Nurr1* (2.8-fold, $p < 0.01$), and *Snca* (4.6-fold, $p < 0.01$). Another subset of highly enriched genes not commonly associated with midbrain dopamine neurons, such as *Anxa1*, *Calb2*, *Chrna6*, *Gch1*, *Grp*, and *Slc10a4* were further analyzed by qPCR, and paired with their Allen Brain Atlas expression profiles (Figure S4A; Lein et al., 2007). These data confirmed their expression in the ventral midbrain and further validate the ability of this approach to identify transcripts expressed in specific subsets of projection neurons.

We also found differential expression of the neurotensin receptor isoforms Ntsr1 and Ntsr2, with significant enrichment of *Ntsr1* (6.1-fold) and depletion of *Ntsr2* (7.4-fold) in the immunoprecipitated RNA. Ntsr1 has been shown previously to play an important role in signaling from the LH to the VTA as part of a reward circuit (Kempadoo et al., 2013). The expression of these isoforms was confirmed by qPCR, with *Ntsr1* enriched 5.4-fold ($p < 0.01$) and *Ntsr2* depleted 8.3-fold ($p < 0.05$; Figure S4C). RNAs for numerous additional genes were significantly enriched in the IP RNA and many of these genes are likely to be markers for populations of neurons projecting to the NAc (Figure S4B). Importantly, when we tested the effect of CAV-GFP infection on expression of a subset of identified marker genes in tissue culture, no substantial alterations were observed (Figure S4D).

Identification of Novel Projection Markers

In our analysis of the RNA-seq data, we observed that a subclass of S100A genes (seven out of eight) were substantially depleted from our immunoprecipitation. However, *S100a10* was significantly enriched (2.1-fold; Figure 5A), and this was confirmed by qPCR (2.1-fold, $p < 0.01$; Figure 5B). *S100a10* expression was not significantly altered by infection with CAV-GFP *in vitro* (Figure S4D). *S100a10*, also known as p11, is known to interact with serotonin receptors and has been causally implicated in depressive disorders (Svenningsson et al., 2006). Indeed, p11-containing cortical projection neurons have recently been identified as being responsible for mediating the response to antidepressants (Schmidt et al., 2012); however, data suggesting a possible role for p11 neurons projecting from hypothalamus to NAc are lacking.

To validate the finding that hypothalamic neurons expressing p11 project to the NAc using a different neural tracer, we generated a replication-deficient pseudorabies virus expressing mCherry (PRV-mCherry). PRV is another well-characterized virus that is retrogradely transported after injection, and similar to CAV-GFP, this strain is incapable of traversing synapses.

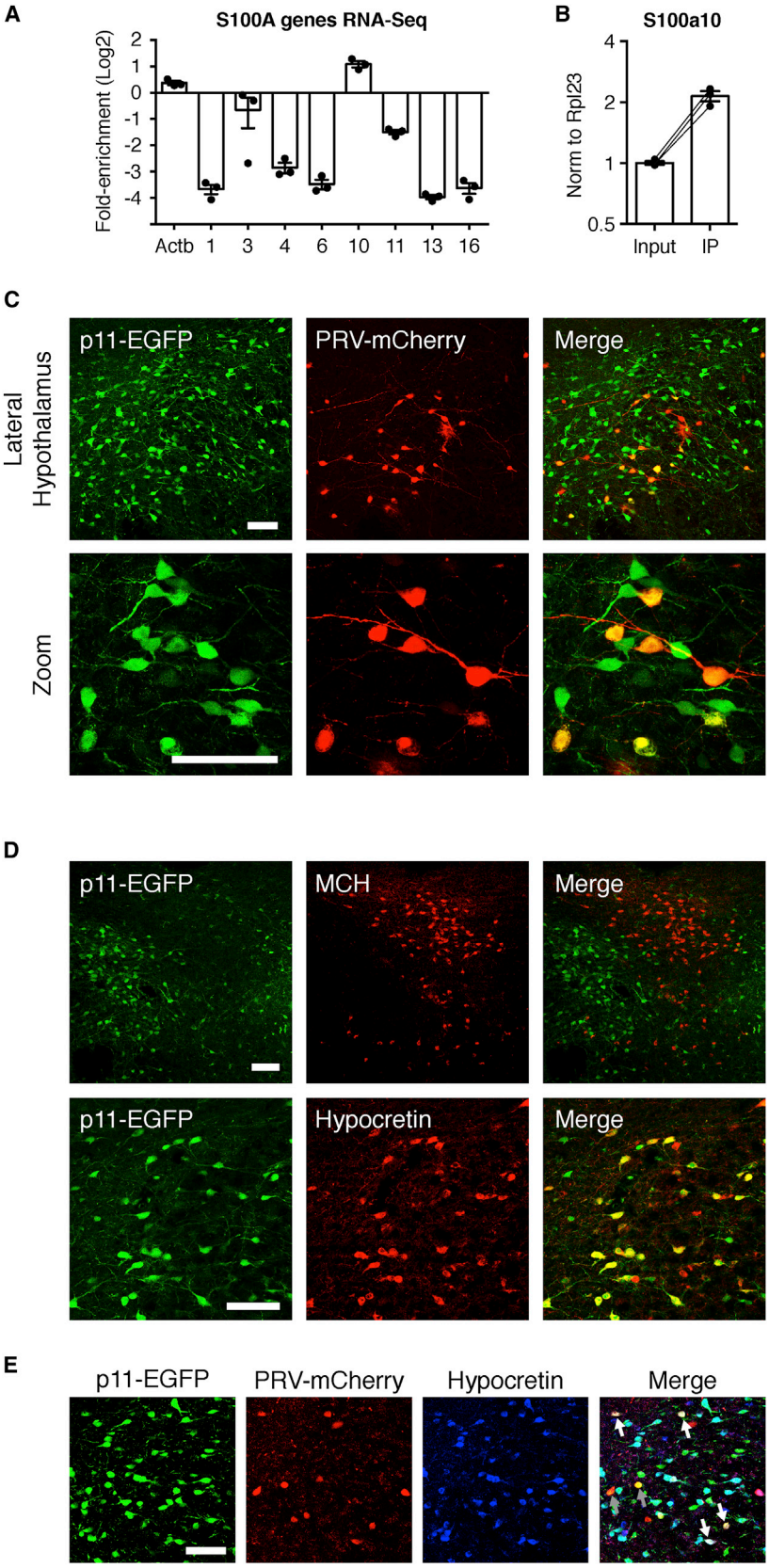

Figure 5. A Subset of Hypothalamic Projection Neurons Express p11

(A) Differential enrichment (IP/Input) of the S100A family of genes in neurons projecting to the nucleus accumbens assessed by RNA-seq, on a Log2 scale. Actin (*Actb*) is shown for reference.

(B) qPCR confirmation of S100a10 (p11) enrichment ($p < 0.01$).

(C) Colocalization between p11-EGFP and PRV-mCherry in the lateral hypothalamus.

(D) Top: colocalization between p11-EGFP and MCH. Bottom: colocalization between p11-EGFP and hypocretin.

(E) Colocalization between p11-EGFP, PRV-mCherry, and hypocretin. White arrows indicate triple-stained cells. Gray arrows indicate p11-positive projection neurons that do not colocalize with hypocretin.

qPCR data are normalized to Rpl23. Data are presented as mean ± SEM. All scale bars, 100 μm. See also Figure S5.

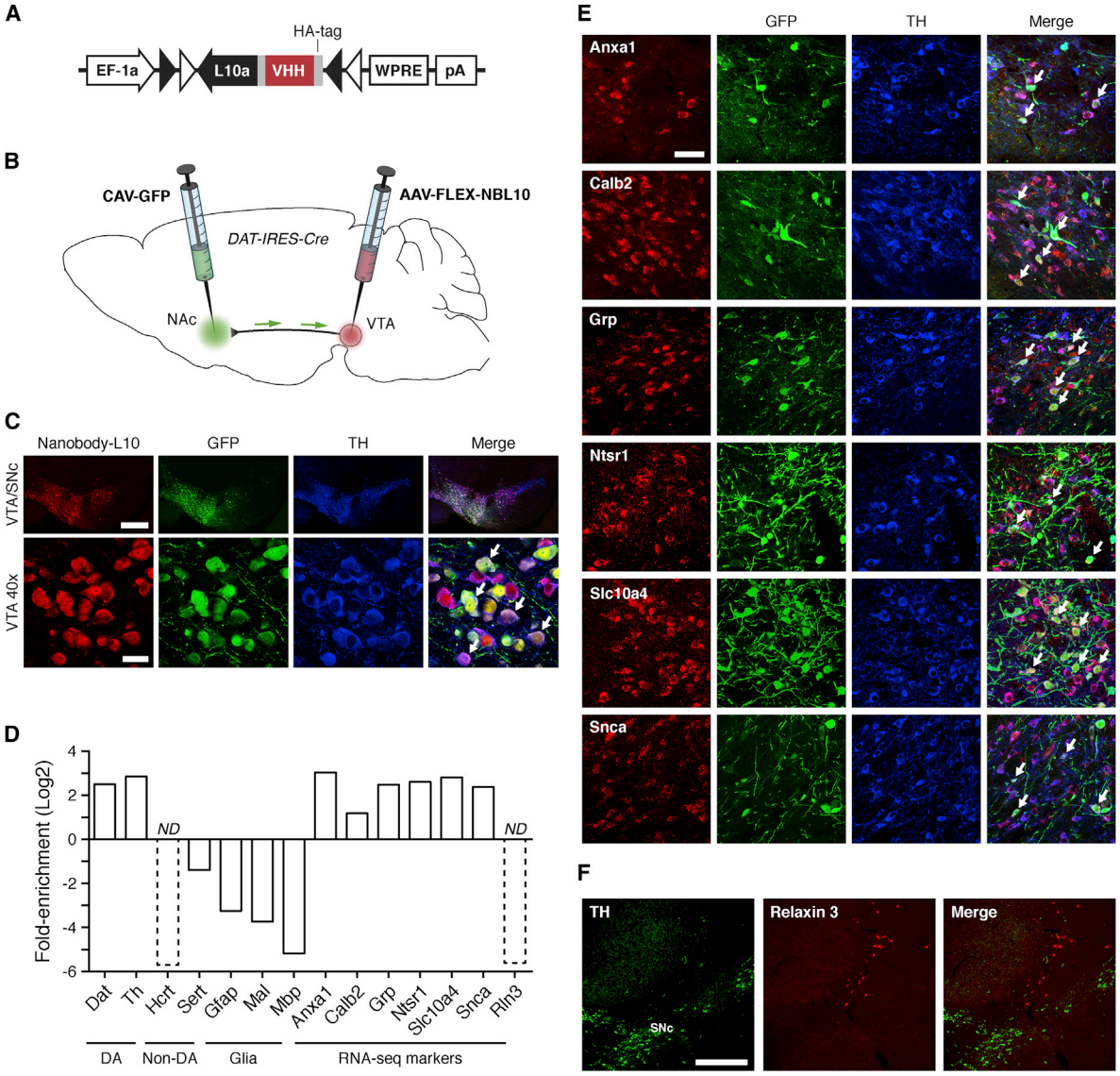

Figure 6. Molecular Profiling of VTA Dopamine Neurons Projecting to the Nucleus Accumbens

(A) AAV-FLEX-NBL10 construct developed to conditionally express NBL10 in the presence of Cre recombinase.

(B) AAV-FLEX-NBL10 is injected into the VTA and CAV-GFP into the NAc of DAT-IRES-Cre mice. NBL10 is restricted to VTA dopamine neurons, and CAV-GFP to NAc-projecting neurons. Only ribosomes from double-labeled cells (VTA dopamine neurons projecting to the NAc) can be immunoprecipitated.

(C) Colocalization between NBL10, GFP (from CAV), and TH in the VTA.

(D) qPCR after cell-type-/projection-specific IPs. Data are expressed as fold enrichment (IP RNA/Input RNA). ND means that IP RNA is not detected.

(E) Enriched marker genes from (D) labeled using FISH. Colocalization between enriched genes, GFP (from CAV), and TH.

(F) Colocalization between Relaxin 3 and TH.

qPCR data are normalized to Rpl23. Scale bars, (top) 500 μm and (bottom) 25 μm in (C), and 50 μm for (E). White arrows in (C) and (E) indicate triple-stained cells.

We injected PRV-mCherry bilaterally into the nucleus accumbens of p11-EGFP transgenic mice (Oh et al., 2013) and observed substantial overlap between cells expressing p11 (EGFP) and mCherry in the lateral hypothalamus (Figure 5C), confirming these neurons project to the NAc.

We additionally wanted to know if there was any overlap between the p11 projection neurons and other markers for cell-types in the lateral hypothalamus that project to the NAc. Costaining for MCH and p11-EGFP revealed clear anatomical segregation between the two cell-types (Figure 5D, top). Furthermore, we were not able to colocalize p11 and MCH in any neurons of the p11-EGFP mouse. These data suggest that the p11 neurons in the LH that project to the NAc comprise a subset of LH neurons distinct from MCH neurons. We noted, however, in the RNA-seq data that there was significant enrichment for hypocretin RNA (9.6-fold; Table S1). Hypocretin expression defines a

distinct subpopulation of lateral hypothalamic neurons that does not overlap with MCH neurons. We thus performed immunohistochemistry for p11 and hypocretin and observed significant overlap and cellular colocalization between the two cell-types (Figure 5D, bottom). We found that p11 was expressed in three different regions of the hypothalamus (the arcuate nucleus, LH, and paraventricular hypothalamus), and overlaps substantially with hypocretin in the LH (Figure S5A). The overlap between p11 and hypocretin in the LH ranged between 39%–52%, depending on the relative position along the AP axis (Figure S5B).

We then injected PRV-mCherry into the nucleus accumbens of p11-EGFP mice and costained for hypocretin. Triple staining for GFP, mCherry, and hypocretin revealed that p11 neurons projecting to the nucleus accumbens partially overlap with the LH hypocretin neurons (Figure 5E). Overall, this study identifies a subpopulation of p11 neurons in the LH that project to the NAc, and demonstrates that most but not all of these projection neurons coexpress hypocretin.

Molecular Profiling of VTA Dopamine Neurons Projecting to Nucleus Accumbens

In our earlier studies, we identified a number of markers that are expressed in ventral midbrain neurons projecting to the nucleus accumbens (see Figure S4). The data did not distinguish whether these markers were expressed in dopaminergic neurons of the VTA or in a different population. To test whether these markers are expressed in VTA dopamine neurons projecting to the nucleus accumbens, we set out to extend the current approach to make it cell-type-specific. To accomplish this, we took advantage of the fact that our technique utilizes a two-component system; namely, both GFP and NBL10 are required to immunoprecipitate RNA from a given cell. Furthermore, the NBL10 construct is relatively small (~1 kb), which makes it amenable to cloning into a Cre-dependent (FLEXed) AAV (Atasoy et al., 2008). We thus cloned the Nanobody-L10 fusion protein (NBL10) into a Cre-conditional AAV (AAV-FLEX-NBL10; Figure 6A). We then injected CAV-GFP into the nucleus accumbens, and AAV-FLEX-NBL10 into the VTA of DAT-IRES-Cre mice (Figure 6B; Bäckman et al., 2006). Immunohistochemistry against NBL10 and TH demonstrated that NBL10 expression was restricted to midbrain dopamine neurons. Furthermore, we noted that a subset of these neurons were also labeled with GFP, confirming that we had targeted a substantial number of VTA dopamine neurons that project to the NAc (Figure 6C).

To purify ribosomes from only those VTA dopamine neurons that project to the NAc, we dissected a 2 mm piece of tissue that included the midbrain and performed IPs as described above. In this case, we precipitated RNA only from VTA dopamine neurons that project to the NAc, as only they will express both GFP and NBL10. Importantly, ribosomes from cells expressing only GFP (nondopamine neurons that project to the NAc) or only NBL10 (VTA dopamine neurons that do not project to the NAc) will not be precipitated, as both components are required. We substantially enriched for midbrain dopamine markers including *Slc6a3* (5.7-fold) and *Th* (7.2-fold), while depleting for nondopaminergic marker genes *Hcrt* (IP RNA did not amplify) and *Slc6a4* (2.6-fold), as well as glial markers *Gfap* (9.5-fold), *Mal* (13.3-fold), and *Mbp* (36-fold) (Figure 6D).

A number of genes identified by our RNA-seq study are expressed in the ventral midbrain (see Allen Brain Atlas and Figure S4), suggesting that these are markers for VTA dopamine neurons projecting to the nucleus accumbens. We assessed the enrichment of seven of these different marker genes by qPCR. Six of the genes were substantially enriched: *Anxa1* (8.2-fold), *Calb2* (2.3-fold), *Grp* (5.6-fold), *Ntsr1* (6.1-fold), *Slc10a4* (7.1-fold), and *Snca* (5.2-fold) (Figure 6D). To further validate that the enriched subset of genes are expressed in VTA dopamine neurons projecting to the NAc, we injected the NAc with CAV-GFP. We then performed fluorescence in situ hybridization (FISH) against each one of these marker genes in tandem with immunohistochemistry against GFP and TH (Figure 6E). In each case, we observed substantial numbers of triple-labeled cells (white arrows), confirming that we were able to profile projective VTA dopamine neurons. Of note, previous studies have shown expression of *Grp* in midbrain dopamine neurons (Chung et al., 2005), though localization to the nucleus accumbens-projecting dopamine neurons has not been demonstrated. Conversely, we did not enrich for relaxin-3 (*Rln3*), which was identified in the RNA-seq study (Figure 6D). Upon costaining for relaxin-3 mRNA and TH, we found that this marker was not expressed in midbrain dopamine neurons, but rather in a discrete population dorsal to the posterior substantia nigra (Figure 6F). Thus, by systematically comparing data generated using AAV-FLEX-NBL10 to the region-specific approach, we were able to identify markers for VTA dopamine neurons, as well as markers for nondopaminergic cell-types.

DISCUSSION

Numerous studies have focused on the comprehensive, high-resolution mapping of the connectivity within the central nervous system (Helmstaedter et al., 2013; Maisak et al., 2013; Takemura et al., 2013). This work, along with studies dating back to the mid-1980s elucidating the connectome of the nematode *C. elegans* (White et al., 1986), have worked toward the important goal of relating neural structure to its function (Lichtman and Denk, 2011; Morgan and Lichtman, 2013). However, connectomic information is necessary but not sufficient to characterize the role of neural populations within a functioning circuit, in part because neural circuitry is labile to neuromodulation, which is essential to its function but invisible to neuroanatomical reconstruction (Bargmann, 2012). Thus, to understand how neural circuits give rise to behavior, the synthesis of connectomic and molecular information is essential.

The identification of markers for specific neurons enables an array of studies delineating their function through use of electrophysiology, molecular profiling, and neural activation/inhibition using optogenetics or chemical genetics (Armbruster et al., 2007; Boyden et al., 2005). Recently, translational profiling approaches have made it possible to profile neurons based on the expression of cell-type-specific marker genes (Heiman et al., 2008), as well as changes in their activity (Knight et al., 2012); however, these approaches do not provide neuroanatomical information about the neurons being profiled. Thus, means for simultaneously generating connectomic and molecular

information would help advance our understanding of how neural circuits give rise to behavior.

Projection-Specific Translational Profiling

GFP is commonly encoded in retrograde tracing viruses to identify presynaptic inputs to a defined locus within the brain. However, while GFP expression can be used to confirm a neuroanatomical connection, it does not reveal the molecular composition of the cell-type. Additionally, many of the retrograde viruses used, such as rabies virus, are often acutely toxic to the cells they infect, potentially altering transcriptomic profiles (Osakada and Callaway, 2013; Wickersham et al., 2007). To enable molecular profiling of a presynaptic cell-type, we required an efficient retrograde virus expressing GFP that had minimal toxicity to the infected cells. Canine adenovirus (CAV) had previously been used for restoration of nigrostriatal dopamine release in a model of dopamine deficiency, demonstrating the long-term preservation of neural function (Hnasko et al., 2006). In this report, we used CAV-GFP to label the soma of projection neurons in which ribosomes were tagged with an anti-GFP nanobody.

We focused our efforts on inputs to the nucleus accumbens (NAc), as they are known to play an important role in such diverse behaviors as feeding (Georgescu et al., 2005), social interaction (Dölen et al., 2013), and reward processing (Lammel et al., 2012). Dysfunction of these neural populations is also implicated in a variety of disease states, such as obesity (Ludwig et al., 2001), addiction (Lüscher and Malenka, 2011), and depression (Chaudhury et al., 2013; Tye et al., 2013).

This work additionally enables the molecular definition of anatomically interspersed populations of neurons within the brain based on their projection pattern. The VTA, for example, is a heterogeneous nucleus with distinct subsets of dopaminergic neurons that can be classified based on their projections to a number of postsynaptic targets such as the medial prefrontal cortex, nucleus accumbens, and hippocampus. However, these populations are not dissociable by manual dissection, making the profiling of these distinct neuronal populations impossible using established techniques such as bacTRAP and RiboTag. Thus, it is likely that molecular profiling of genetically defined projective cell-types will be an important application of projection-specific translational profiling. Indeed, it is already becoming clear that different projections from a molecularly defined nucleus can have differential behavioral effects relevant to reward processing (Lammel et al., 2012), as well as depression (Chaudhury et al., 2013). Toward this end, we extended the current approach to profile VTA dopamine neurons projecting to the nucleus accumbens using CAV-GFP, and a Cre-driver line with an AAV that we generated.

The data reported here further indicate that NBL10 could be incorporated into other vector systems for a variety of studies. For example, a monosynaptic rabies virus expressing GFP could be used in tandem with the SYN-NBL10 mouse (crossed to a Cre-driver line) to profile neurons synapsing onto a molecularly defined postsynaptic target (see Wall et al., 2013). Similarly, this system could be adapted to identify markers for neurons postsynaptic to genetically defined cells using Cre-dependent anterograde strains of herpes simplex virus (Lo and Anderson, 2011).

Molecularly profiling neurons based on their pattern of connectivity represents a methodology that is conceptually distinct from a number of recent efforts, which have been made to obtain molecular genetic information from connectomic-based experiments. Approaches such as single-synapse proteomic analysis (Micheva et al., 2010) and the Allen Brain Institute's cell-type-specific, virally targeted expression of GFP (connectivity.brain-map.org) have made significant progress in this area; however, these methodologies require either highly sensitive microscopy methods or numbers of transgenic mouse lines expressing Cre recombinase. Additionally, these approaches require an a priori defined cell-type to be targeted. Thus, an unbiased approach to studying molecular connectivity within the brain as reported here should be of general use.

Alternate strategies have also been employed to molecularly profile neurons based on their projection pattern, particularly within the VTA. However, these approaches such as laser capture microdissection (Lammel et al., 2008; Li et al., 2013) have low RNA yields, require specialized instrumentation and are difficult to implement, and are therefore not amenable to high-throughput analyses. Another possible approach to projection-specific molecular profiling would be through fluorescence-activated cell sorting (FACS) of retrogradely-labeled, fluorophore-positive neurons (see Sugino et al., 2006); however, the current isolation protocols for neuronal FACS (Lobo et al., 2006) appear to induce cellular stress, and the resulting molecular profiles have reduced sensitivity in comparison to techniques like bacTRAP. Projection-specific translational profiling using TRAP-based methodologies, therefore, allows for access to translating mRNAs with high efficiency, enabling detailed molecular analyses using quantitative PCR and RNA-seq.

Intersectional Genetic Applications of NBL10-Based TRAP

The NBL10-based approach could be engineered to further molecularly refine subpopulations of neural cell-types defined by the intersection of two markers. For example, to translationally profile a neural cell-type defined by two marker genes (e.g., genes A and B), one could drive expression of NBL10 on the gene A promoter, and cross this mouse to a gene B-GFP mouse. This particular approach would allow for increasing granularity in the systematic analysis of CNS cell-types that are currently characterized by a single marker gene. Furthermore, AAV-FLEX-NBL10 could be used for this purpose, as well. A GFP line could be crossed to a partially overlapping Cre-driver line, and the offspring could be injected with AAV-FLEX-NBL10 to profile the intersection of these two cell types. The data reported here indicate that this approach is feasible and would potentially enable an intersectional strategy for molecular profiling of neurons allowing a further refinement of the analysis of a variety of neuronal subpopulations.

EXPERIMENTAL PROCEDURES

Animals

All experiments performed were approved by the Rockefeller University Institutional Animal Care and Use Committee and were in accordance with

the National Institutes of Health guidelines. SYN-NBL10 mice were generated and maintained at Rockefeller University. A fragment encoding the Nanobody-L10 fusion was synthesized and cloned into pSynAmp to generate pSynAmp-Nano-L10. pSynAmp-Nano-L10 was linearized and injected into FVB zygotes to generate SYN-NBL10 mice. See Extended Experimental Procedures for details. Animals used in the study were male and female wild-type, SYN-NBL10, p11-EGFP transgenic, or DAT-IRES-Cre knockin mice 10–20 weeks old at the time of sacrifice. All mice were housed on a 12 hr light-dark schedule and were sacrificed between the same circadian period (12:00–16:00).

Construction of AAV-FLEX-NBL10

NBL10 was PCR amplified from SYN-NBL10 genomic DNA with primers adding a 5′ HA epitope tag, along with restriction sites for subcloning into an AAV vector. The PCR product was cloned in the reverse orientation into the AscI and NheI sites of pAAV-EF1a-DIO-hChR2(H134R)-mCherry (Addgene 20297) generating pAAV-FLEX-NBL10. The plasmid was then sent to the University of North Carolina Vector Core for AAV packaging with serotype 5.

Stereotaxic Surgeries

SYN-NBL10 transgenic, p11-EGFP, or wild-type mice 8–18 weeks of age were induced and maintained on isofluorane anesthesia before being bilaterally injected with 0.5 μl CAV-GFP or PRV-mCherry in the nucleus accumbens shell (NAc, coordinates: ± 1.0 mm ML, +1.35 mm AP, −4.2 mm DV). DAT-IRES-Cre mice were injected in both the NAc with CAV-GFP, as well as the VTA with AAV-FLEX-NBL10 (coordinates: ± 0.5 mm ML, −3.15 mm AP, −4.2 mm DV). ML and AP coordinates are relative to bregma and DV coordinates are relative to the pial surface. After viral injections, the needle was left in place for 10 min before slowly retracting. The skin was closed with a surgical clip.

Immunohistochemistry

Brain sections were stained and mounted, followed by imaging on a Zeiss LSM780 confocal microscope. Further details can be found in Extended Experimental Procedures.

GFP Immunoprecipitations

Fourteen days after injections, mice were sacrificed and the ventral midbrain and posterior hypothalamus were rapidly dissected on ice. Briefly, a 3 mm slice was made approximately covering the region 1–4 mm posterior to bregma. Lateral and dorsal parts were removed to isolate hypothalamus and the ventral midbrain. Brains were then pooled into three groups of six mice per group, homogenized in the presence of recombinant nanobody (100 ng/ml, ChromoTek), and centrifuged to clarify. GFP Immunoprecipitation was performed with two mouse monoclonal antibodies (19C8, 19F7; Doyle et al., 2008). The resulting RNA was purified using the Absolutely RNA Nanoprep Kit (Agilent) and analyzed using an Agilent 2100 Bioanalyzer, followed by reverse transcription (QIAGEN QuantiTect) and Taqman qPCR. Libraries for RNA-seq were prepared with oligo dT priming using the SMARTer Ultra Low RNA Kit (Clontech) and analyzed on an Illumina HiSeq 2500. Further details can be found in Extended Experimental Procedures.

Statistics

Transcript abundance estimates and differential expression tests for RNA-seq data were performed with cufflinks (cuffdiff). All other statistics were performed in Prism GraphPad.

ACCESSION NUMBERS

The GEO accession number for the RNA-seq data reported in this paper is GSE55800.

SUPPLEMENTAL INFORMATION

Supplemental Information includes Extended Experimental Procedures, five figures, and one table and can be found with this article online at http://dx.doi.org/10.1016/j.cell.2014.03.059.

AUTHOR CONTRIBUTIONS

M.I.E. and A.R.N. contributed equally to this paper. Order of authorship was determined alphabetically. A.R.N. and M.I.E. designed and performed all experiments. Z.A.K. generated the SYN-NBL10 mouse, L.E.P. generated PRV-mCherry, and K.N.L. performed IHC. A.R.N., M.I.E., and J.M.F. analyzed data and wrote the paper.

ACKNOWLEDGMENTS

This work was supported by the Howard Hughes Medical Institute, the JPB Foundation, and NIDA grant 1RO1DA018799-01 (J.M.F.). Z.A.K. acknowledges support from the New York Stem Cell Foundation, the Klingenstein Fund, Sloan Foundation, the McKnight Foundation, and the Brain and Behavior Research Foundations. We thank Scott Dewell and the Rockefeller University Genomics Core for help with RNA-seq and bioinformatics, and Ana Milosevic, Yong Kim, and Paul Greengard for contributing p11-EGFP mice. We thank Karl Deisseroth for contributing the plasmid pAAV-EF1a-DIO-hChR2(H134R)-mCherry (Addgene 20297), which was used in the creation of AAV-FLEX-NBL10. We also thank Eric F. Schmidt for helpful discussions. Imaging was performed at the Rockefeller University Bio-Imaging Resource Center. CAV-GFP was obtained from the Montpellier vector platform.

Received: October 29, 2013
Revised: February 5, 2014
Accepted: March 14, 2014
Published: May 22, 2014

REFERENCES

Armbruster, B.N., Li, X., Pausch, M.H., Herlitze, S., and Roth, B.L. (2007). Evolving the lock to fit the key to create a family of G protein-coupled receptors potently activated by an inert ligand. Proc. Natl. Acad. Sci. USA *104*, 5163–5168.

Atasoy, D., Aponte, Y., Su, H.H., and Sternson, S.M. (2008). A FLEX switch targets Channelrhodopsin-2 to multiple cell types for imaging and long-range circuit mapping. J. Neurosci. *28*, 7025–7030.

Bäckman, C.M., Malik, N., Zhang, Y., Shan, L., Grinberg, A., Hoffer, B.J., Westphal, H., and Tomac, A.C. (2006). Characterization of a mouse strain expressing Cre recombinase from the 3′ untranslated region of the dopamine transporter locus. Genesis *44*, 383–390.

Bargmann, C.I. (2012). Beyond the connectome: how neuromodulators shape neural circuits. Bioessays *34*, 458–465.

Boyden, E.S., Zhang, F., Bamberg, E., Nagel, G., and Deisseroth, K. (2005). Millisecond-timescale, genetically targeted optical control of neural activity. Nat. Neurosci. *8*, 1263–1268.

Bru, T., Salinas, S., and Kremer, E.J. (2010). An update on canine adenovirus type 2 and its vectors. Viruses *2*, 2134–2153.

Chaudhury, D., Walsh, J.J., Friedman, A.K., Juarez, B., Ku, S.M., Koo, J.W., Ferguson, D., Tsai, H.C., Pomeranz, L., Christoffel, D.J., et al. (2013). Rapid regulation of depression-related behaviours by control of midbrain dopamine neurons. Nature *493*, 532–536.

Chung, C.Y., Seo, H., Sonntag, K.C., Brooks, A., Lin, L., and Isacson, O. (2005). Cell type-specific gene expression of midbrain dopaminergic neurons reveals molecules involved in their vulnerability and protection. Hum. Mol. Genet. *14*, 1709–1725.

Croizier, S., Franchi-Bernard, G., Colard, C., Poncet, F., La Roche, A., and Risold, P.Y. (2010). A comparative analysis shows morphofunctional differences between the rat and mouse melanin-concentrating hormone systems. PLoS ONE *5*, e15471.

Dölen, G., Darvishzadeh, A., Huang, K.W., and Malenka, R.C. (2013). Social reward requires coordinated activity of nucleus accumbens oxytocin and serotonin. Nature *501*, 179–184.

Doyle, J.P., Dougherty, J.D., Heiman, M., Schmidt, E.F., Stevens, T.R., Ma, G., Bupp, S., Shrestha, P., Shah, R.D., Doughty, M.L., et al. (2008). Application of a translational profiling approach for the comparative analysis of CNS cell types. Cell *135*, 749–762.

Georgescu, D., Sears, R.M., Hommel, J.D., Barrot, M., Bolaños, C.A., Marsh, D.J., Bednarek, M.A., Bibb, J.A., Maratos-Flier, E., Nestler, E.J., and DiLeone, R.J. (2005). The hypothalamic neuropeptide melanin-concentrating hormone acts in the nucleus accumbens to modulate feeding behavior and forced-swim performance. J. Neurosci. *25*, 2933–2940.

Heiman, M., Schaefer, A., Gong, S., Peterson, J.D., Day, M., Ramsey, K.E., Suárez-Fariñas, M., Schwarz, C., Stephan, D.A., Surmeier, D.J., et al. (2008). A translational profiling approach for the molecular characterization of CNS cell types. Cell *135*, 738–748.

Helmstaedter, M., Briggman, K.L., Turaga, S.C., Jain, V., Seung, H.S., and Denk, W. (2013). Connectomic reconstruction of the inner plexiform layer in the mouse retina. Nature *500*, 168–174.

Hnasko, T.S., Perez, F.A., Scouras, A.D., Stoll, E.A., Gale, S.D., Luquet, S., Phillips, P.E., Kremer, E.J., and Palmiter, R.D. (2006). Cre recombinase-mediated restoration of nigrostriatal dopamine in dopamine-deficient mice reverses hypophagia and bradykinesia. Proc. Natl. Acad. Sci. USA *103*, 8858–8863.

Kempadoo, K.A., Tourino, C., Cho, S.L., Magnani, F., Leinninger, G.M., Stuber, G.D., Zhang, F., Myers, M.G., Deisseroth, K., de Lecea, L., and Bonci, A. (2013). Hypothalamic neurotensin projections promote reward by enhancing glutamate transmission in the VTA. J. Neurosci. *33*, 7618–7626.

Knight, Z.A., Tan, K., Birsoy, K., Schmidt, S., Garrison, J.L., Wysocki, R.W., Emiliano, A., Ekstrand, M.I., and Friedman, J.M. (2012). Molecular profiling of activated neurons by phosphorylated ribosome capture. Cell *151*, 1126–1137.

Lammel, S., Hetzel, A., Häckel, O., Jones, I., Liss, B., and Roeper, J. (2008). Unique properties of mesoprefrontal neurons within a dual mesocorticolimbic dopamine system. Neuron *57*, 760–773.

Lammel, S., Ion, D.I., Roeper, J., and Malenka, R.C. (2011). Projection-specific modulation of dopamine neuron synapses by aversive and rewarding stimuli. Neuron *70*, 855–862.

Lammel, S., Lim, B.K., Ran, C., Huang, K.W., Betley, M.J., Tye, K.M., Deisseroth, K., and Malenka, R.C. (2012). Input-specific control of reward and aversion in the ventral tegmental area. Nature *491*, 212–217.

Lein, E.S., Hawrylycz, M.J., Ao, N., Ayres, M., Bensinger, A., Bernard, A., Boe, A.F., Boguski, M.S., Brockway, K.S., Byrnes, E.J., et al. (2007). Genome-wide atlas of gene expression in the adult mouse brain. Nature *445*, 168–176.

Li, X., Qi, J., Yamaguchi, T., Wang, H.L., and Morales, M. (2013). Heterogeneous composition of dopamine neurons of the rat A10 region: molecular evidence for diverse signaling properties. Brain Struct. Funct. *218*, 1159–1176.

Lichtman, J.W., and Denk, W. (2011). The big and the small: challenges of imaging the brain's circuits. Science *334*, 618–623.

Lim, B.K., Huang, K.W., Grueter, B.A., Rothwell, P.E., and Malenka, R.C. (2012). Anhedonia requires MC4R-mediated synaptic adaptations in nucleus accumbens. Nature *487*, 183–189.

Lo, L., and Anderson, D.J. (2011). A Cre-dependent, anterograde transsynaptic viral tracer for mapping output pathways of genetically marked neurons. Neuron *72*, 938–950.

Lobo, M.K., Karsten, S.L., Gray, M., Geschwind, D.H., and Yang, X.W. (2006). FACS-array profiling of striatal projection neuron subtypes in juvenile and adult mouse brains. Nat. Neurosci. *9*, 443–452.

Ludwig, D.S., Tritos, N.A., Mastaitis, J.W., Kulkarni, R., Kokkotou, E., Elmquist, J., Lowell, B., Flier, J.S., and Maratos-Flier, E. (2001). Melanin-concentrating hormone overexpression in transgenic mice leads to obesity and insulin resistance. J. Clin. Invest. *107*, 379–386.

Lüscher, C., and Malenka, R.C. (2011). Drug-evoked synaptic plasticity in addiction: from molecular changes to circuit remodeling. Neuron *69*, 650–663.

Maisak, M.S., Haag, J., Ammer, G., Serbe, E., Meier, M., Leonhardt, A., Schilling, T., Bahl, A., Rubin, G.M., Nern, A., et al. (2013). A directional tuning map of Drosophila elementary motion detectors. Nature *500*, 212–216.

Micheva, K.D., Busse, B., Weiler, N.C., O'Rourke, N., and Smith, S.J. (2010). Single-synapse analysis of a diverse synapse population: proteomic imaging methods and markers. Neuron *68*, 639–653.

Morgan, J.L., and Lichtman, J.W. (2013). Why not connectomics? Nat. Methods *10*, 494–500.

Mosharov, E.V., Larsen, K.E., Kanter, E., Phillips, K.A., Wilson, K., Schmitz, Y., Krantz, D.E., Kobayashi, K., Edwards, R.H., and Sulzer, D. (2009). Interplay between cytosolic dopamine, calcium, and α-synuclein causes selective death of substantia nigra neurons. Neuron *62*, 218–229.

Muyldermans, S. (2013). Nanobodies: natural single-domain antibodies. Annu. Rev. Biochem. *82*, 775–797.

Oh, Y.S., Gao, P., Lee, K.W., Ceglia, I., Seo, J.S., Zhang, X., Ahn, J.H., Chait, B.T., Patel, D.J., Kim, Y., and Greengard, P. (2013). SMARCA3, a chromatin-remodeling factor, is required for p11-dependent antidepressant action. Cell *152*, 831–843.

Osakada, F., and Callaway, E.M. (2013). Design and generation of recombinant rabies virus vectors. Nat. Protoc. *8*, 1583–1601.

Ries, J., Kaplan, C., Platonova, E., Eghlidi, H., and Ewers, H. (2012). A simple, versatile method for GFP-based super-resolution microscopy via nanobodies. Nat. Methods *9*, 582–584.

Rothbauer, U., Zolghadr, K., Tillib, S., Nowak, D., Schermelleh, L., Gahl, A., Backmann, N., Conrath, K., Muyldermans, S., Cardoso, M.C., and Leonhardt, H. (2006). Targeting and tracing antigens in live cells with fluorescent nanobodies. Nat. Methods *3*, 887–889.

Sanz, E., Yang, L., Su, T., Morris, D.R., McKnight, G.S., and Amieux, P.S. (2009). Cell-type-specific isolation of ribosome-associated mRNA from complex tissues. Proc. Natl. Acad. Sci. USA *106*, 13939–13944.

Schmidt, E.F., Warner-Schmidt, J.L., Otopalik, B.G., Pickett, S.B., Greengard, P., and Heintz, N. (2012). Identification of the cortical neurons that mediate antidepressant responses. Cell *149*, 1152–1163.

Sesack, S.R., and Grace, A.A. (2010). Cortico-Basal Ganglia reward network: microcircuitry. Neuropsychopharmacology *35*, 27–47.

Silva, J.P., von Meyenn, F., Howell, J., Thorens, B., Wolfrum, C., and Stoffel, M. (2009). Regulation of adaptive behaviour during fasting by hypothalamic Foxa2. Nature *462*, 646–650.

Stanley, S.A., Domingos, A.I., Kelly, L., Garfield, A., Damanpour, S., Heisler, L., and Friedman, J. (2013). Profiling of glucose-sensing neurons reveals that GHRH neurons are activated by hypoglycemia. Cell Metab. *18*, 596–607.

Sugino, K., Hempel, C.M., Miller, M.N., Hattox, A.M., Shapiro, P., Wu, C., Huang, Z.J., and Nelson, S.B. (2006). Molecular taxonomy of major neuronal classes in the adult mouse forebrain. Nat. Neurosci. *9*, 99–107.

Svenningsson, P., Chergui, K., Rachleff, I., Flajolet, M., Zhang, X., El Yacoubi, M., Vaugeois, J.M., Nomikos, G.G., and Greengard, P. (2006). Alterations in 5-HT1B receptor function by p11 in depression-like states. Science *311*, 77–80.

Takemura, S.Y., Bharioke, A., Lu, Z., Nern, A., Vitaladevuni, S., Rivlin, P.K., Katz, W.T., Olbris, D.J., Plaza, S.M., Winston, P., et al. (2013). A visual motion detection circuit suggested by Drosophila connectomics. Nature *500*, 175–181.

Tang, J.C., Szikra, T., Kozorovitskiy, Y., Teixiera, M., Sabatini, B.L., Roska, B., and Cepko, C.L. (2013). A nanobody-based system using fluorescent proteins as scaffolds for cell-specific gene manipulation. Cell *154*, 928–939.

Tsien, R.Y. (1998). The green fluorescent protein. Annu. Rev. Biochem. *67*, 509–544.

Tye, K.M., Mirzabekov, J.J., Warden, M.R., Ferenczi, E.A., Tsai, H.C., Finkelstein, J., Kim, S.Y., Adhikari, A., Thompson, K.R., Andalman, A.S., et al. (2013). Dopamine neurons modulate neural encoding and expression of depression-related behaviour. Nature *493*, 537–541.

Wall, N.R., Wickersham, I.R., Cetin, A., De La Parra, M., and Callaway, E.M. (2010). Monosynaptic circuit tracing in vivo through Cre-dependent targeting and complementation of modified rabies virus. Proc. Natl. Acad. Sci. USA *107*, 21848–21853.

Wall, N.R., De La Parra, M., Callaway, E.M., and Kreitzer, A.C. (2013). Differential innervation of direct- and indirect-pathway striatal projection neurons. Neuron *79*, 347–360.

White, J.G., Southgate, E., Thomson, J.N., and Brenner, S. (1986). The structure of the nervous system of the nematode Caenorhabditis elegans. Philos. Trans. R. Soc. Lond. B Biol. Sci. *314*, 1–340.

Wickersham, I.R., Finke, S., Conzelmann, K.K., and Callaway, E.M. (2007). Retrograde neuronal tracing with a deletion-mutant rabies virus. Nat. Methods *4*, 47–49.